Transportation Geotechnics 42 (2023) 101111

Contents lists available at ScienceDirect

Transportation Geotechnics

journal homepage: www.elsevier.com/locate/trgeo

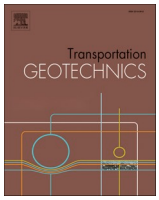

Alteration of soil structure following seepage-induced internal erosion in model infrastructure embankments

I. Johnston [a,b,c,*], W. Murphy [a], J. Holden [c]

[a] School of Earth and Environment, University of Leeds, Leeds LS2 9JT, UK
[b] School of Civil Engineering, University of Leeds, Leeds LS2 9JT, UK
[c] water@leeds, School of Geography, University of Leeds, Leeds LS2 9JT, UK

ARTICLE INFO

Keywords:
Internal Erosion
Embankment
Flooding
Suffusion
Seepage
Rail infrastructure

ABSTRACT

The flooding of infrastructure embankments has the potential to cause lasting destabilisation through seepage-driven internal erosion development. To understand the effects of such erosion on slope behaviour it is imperative to identify where in slopes material alteration most commonly occurs. Laboratory testing on scale models of transportation embankments was undertaken to identify the locations within slopes where material movement, and likely property alteration occurs, caused by seepage through slopes. Changes in material properties were most commonly found to occur along the base of slopes and in regions of slopes adjacent to water inflow. Slope toes were found to have a greater proportion of fine material than elsewhere, with the mean grain size of the slope toe region 4.5% smaller and the coefficient of curvature 9% higher than in the main slope body, suggesting the development of a low permeability region towards the slope toe. The source zone for material deposited at the toe of slopes was the section of slopes adjacent to water inflow and the base of slopes away from the toe, shown by a coarsening of sediment in these zones. Material alteration following flooding was best identified using a combination of coefficient of curvature and mean grain size data. These results have implications for the stability of earthworks during and after flood events, and for the design of earthwork inspection and maintenance regimes.

Introduction

Transport embankment failures following flooding are relatively common globally (e.g. [25,28]). These embankments are often not designed for water impoundment, yet large volumes of ponding can develop when linear earthworks are constructed along the base of slopes and on floodplains (e.g. [22,4]). Sometimes these slopes fail in the aftermath of flood events (e.g. [30]). However, for slopes which remain intact after an individual flood event, there is evidence that flooding and cyclic wetting–drying leads to long-term weakening [27,13,21]. Understanding the lasting alterations in material properties caused by flood-induced processes in sections of slope which are affected by flooding is key to understanding of the potential changes in slope stability and for developing techniques for increasing the flood resilience of slopes. This is especially important given the effects of climate change, in particular the widespread increases in rainfall and flooding which are expected to occur [10], and given that more infrastructure is likely to be developed to support the world's burgeoning population.

Floodwater impoundment behind transportation embankments can cause acute destabilisation through processes including saturation and pore pressure increase, loading and rapid draw down [13]. In addition, seepage-induced internal erosion, scour and cyclic wetting-drying [3,27] cause lasting alterations to slope stability through changes to slope structure and changes in material properties including strength, stiffness and permeability [6,14]. Internal erosion processes, including suffusion and piping, cause the movement of fine particles through slopes. The locations of fine particle loss and accretion are key to determining locations of material property change in slopes after flood recession. Internal erosion of slopes develops in response to flood ponding when there is a hydraulic gradient and sufficient associated water flow within soils and sediments, creating fine particle migration [32].

Previous studies which assessed the effects of flooding on model slopes used spherical silica beads with a bimodal distribution to identify the predominant locations of slope property changes (e.g. [12]). Fine particle movement, measured using average grain size reductions, was

* Corresponding author at: School of Earth and Environment, University of Leeds, Leeds LS2 9JT, UK.
E-mail address: i.g.johnston@leeds.ac.uk (I. Johnston).

https://doi.org/10.1016/j.trgeo.2023.101111
Received 1 May 2023; Received in revised form 15 September 2023; Accepted 17 September 2023
Available online 18 September 2023

found to be predominantly below the phreatic line and towards the base and toe of slopes, under the effects of seepage and gravity [12]. Reductions in average grain size of the material can be considered material 'fining', whereas increases in the average grain size are 'coarsening'. The bimodal grain size distribution of materials used in tests of model slopes with silica grains does not allow for the full development of processes occurring in full-scale slopes comprised of normally graded materials, thus results may not be consistent with graded materials. The fining identified by Horikoshi and Takahashi [12] in lower portions of slopes constructed of silica grains is consistent with observations from seepage flow tests undertaken using permeameters and triaxial apparatus which found that fining occurs towards the seepage outflow (e.g. [15,6]). Triaxial testing has also shown reductions in soil strength behaviour (e.g. [26,19]) and stiffness [2,16] following internal erosion development in soils. Given that these small-scale laboratory tests show that the migration of particles causes property alterations, it is important to understand how this behaviour occurs in up-scaled scenarios.

In addition to average grain size and fines distribution change, it is important to consider the effects of seepage on material indices including coefficient of curvature (*Cc*) and coefficient of uniformity (*Cu*) (Equations 1 and 2) in addition to the effects of particle migration on average grain size.

$$Cu = D_{60}/D_{10} \tag{1}$$

$$Cc = D_{30}^2/(D_{10}D_{60}) \tag{2}$$

Cu and *Cc* are commonly used to determine the gradation and engineering suitability of soils for embankment construction. UIC 719R, the high-speed rail embankment material specification given by the International Union of Railways, requires $1 < Cc < 3$ and $Cu > 6$.

Using a laboratory model of a slope, we aim to increase understanding of where particle movement and fines redistribution is likely to occur in slopes constructed of materials representing those used in embankment construction when subjected to flood simulation loading. Additionally, we assess how seepage and particle movement cause spatially distributed changes in the values of the key material grading parameters, *Cc* and *Cu*.

Methods

Model slopes, replicating a truncated embankment cross section, were constructed (Fig. 1) using material comprising well-graded silts-gravels which met grain size criteria stipulated in UIC719R [29]. Model slopes were used to enable higher relative durations of seepage through slopes, representing longer-term flood conditions, in comparison to sampling full-scale embankments where particle migration would likely take longer to develop. Materials with a realistic grain size distribution and properties representing embankment specifications were used to create a more accurate model of fine particle behaviour, especially in the slope toe region, with the acceptance that this may cause more inter-test variability.

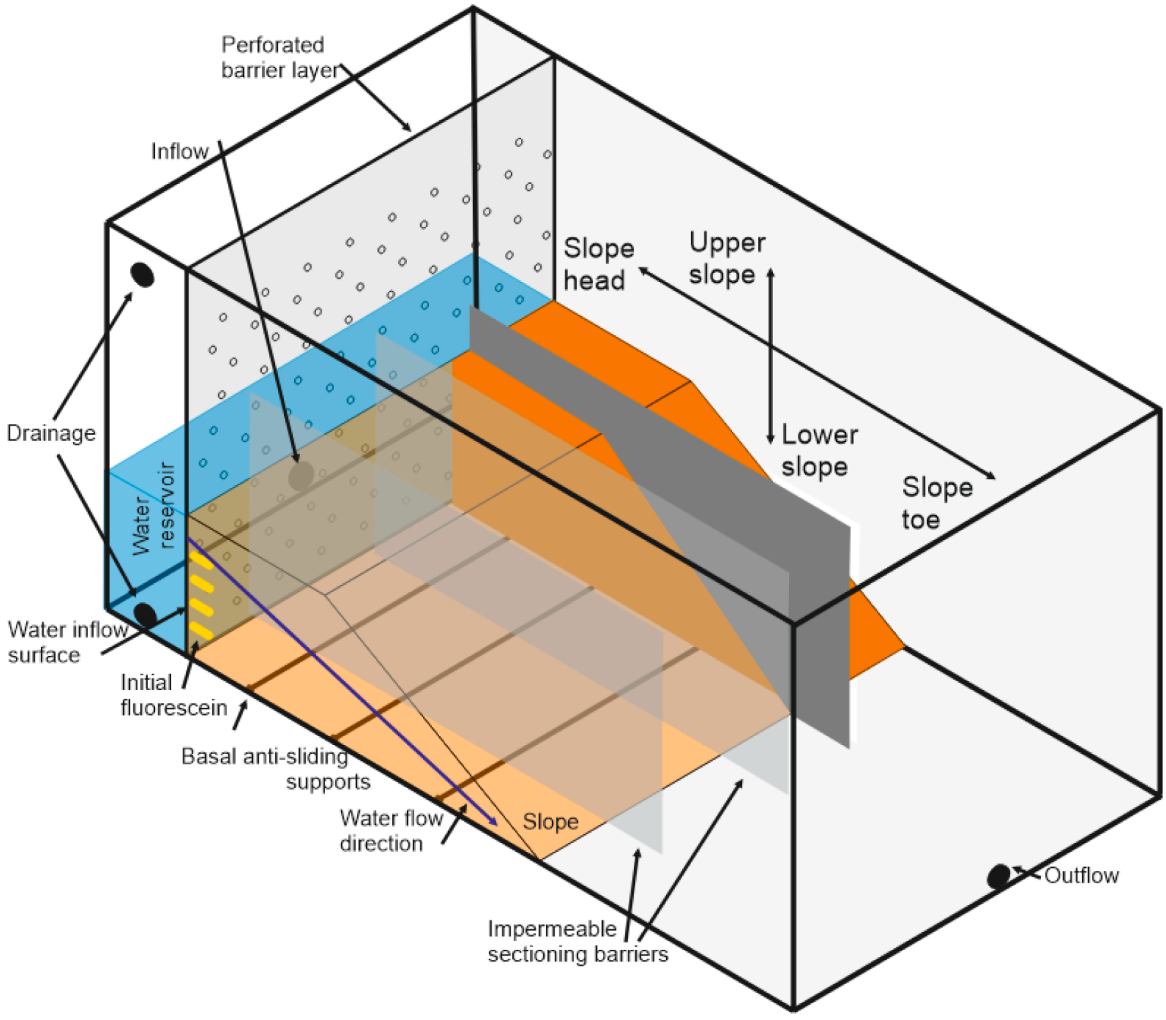

Fig. 1. Experiment design schematic for constructed model slopes. Impermeable section barriers were not present in slopes A, B or E and basal anti-sliding supports were not present in slopes D or E.

Equipment design and slope structure

In total, five slopes (denoted A-E) were constructed. Each slope was constructed in a transparent Perspex box, to allow for observation of slope behaviour during seepage. Slopes were designed to represent one side of an embankment and were 170 mm high, 400 mm long and up to 480 mm wide. Slope dimensions were selected to create a slope angle commensurate with full-scale embankments. Slopes were split into two sections: a flat topped section representing an embankment crest at the head of the slope and a frontal slope section with a slope angle of ~33°. Wooden basal supports were installed to prevent basal sliding between the Perspex box and soil material in slopes A-C (Table 1); these were not used in slopes D and E to ensure that there was no disruption to fluid flow along the base of slopes. Longitudinal supports ran continuously across the full width of slopes, whereas spikes were discontinuous. A fluid reservoir was located behind a permeable Perspex sheet divider at the back of the slope. Seepage into the back of the slope occurred through a series of holes with a grid spacing of 50 mm and 4 mm diameter, to represent infiltration of water during a flood event. The internal faces of the Perspex box were rough, helping to prevent preferential seepage flow between the soil - box contact. No preferential seepage was observed along this interface during the experiments.

For each test, a slope was constructed using moist compaction with lifts of 25 mm between compactions; slopes were constructed with a target density of 1550 kg m^{-3} (Table 1). Moist compaction was utilised to prevent fines separation during the construction processes [18]. The development of seepage through slopes was established via the use of fluorescein powder which was inserted at multiple depths at the head of slopes during compaction and used to track fluid and particle movement. Fluorescein powder is water soluble and allowed the progression of seepage to be tracked through model slopes when illuminated with UV light, as the slope material lacked organic matter and was therefore considered non-acidic [23]. The powder is soluble and therefore it does not alter the soil behaviour during seepage. The development of fluorescence across the length of a model slope showed that seepage was developing through a slope. Throughout the duration of tests, the fluorescein response weakened due to dilution from additional seepage water inflow and was not consistently visible towards the toe of the slopes. Water which seeped through the slope drained via a drainage hole in the Perspex beyond the slope base.

In slopes A, B and E, continuous slopes were constructed without dividers (Fig. 1). In slopes C and D, impermeable dividing barriers were inserted into the slopes parallel to flow (Fig. 1) to create up to four testing transects which could have independent seepage durations – allowing the time-dependent development of particle migration during seepage to be identified for the same slope. In slope C, transect *C-i)* underwent the least seepage at 135 min, with each additional transect undergoing an additional 135 min of seepage. After the requisite time, the inflow seepage holes were blocked to prevent further seepage into a transect – preserving the material in state until the end of the test. In slope D, transect *D-i* underwent no seepage and is a control section.

Table 1
Slope design properties and seepage conditions. Slope density was not available for slope A.

Slope	Mean slope density, *kg* m^{-3}	Seepage duration, *mins*	Hydraulic gradient, *i*	Sampling	Slope structure
A	–	85	3	Nine samples per transect; three transects. Samples from all transects had the same seepage volume.	Longitudinal basal supports
B	1483	246	1	10 samples per transect; three transects. Samples from all transects had the same seepage volume.	Basal spikes
C	1532	135–552	1	10 samples per transect; four transects. Transects were sampled every 135 min, having undergone progressively longer seepage durations.	Three slope dividers Basal spikes
D	1578	0–145	3	10 samples per transect; two transects. Transects sampled after 0 and 135 min.	Three slope dividers
E	1517	374	1	24 samples from a single transect. All samples taken at end of test.	Single narrow slice

Slope material

Granular soils were reconstituted to form a material with the desired grain size distribution and properties. Soils used were produced by mixing two bulk soils with a known grain size distribution. Soil gradation curves are shown in Fig. 2. Material stability was assessed using the stability criteria (Table 2) prescribed by Kenney and Lau [17] which dictate that soils with a h/f value > 1.3 are stable and a h/f value of 1–1.3 indicates a soil in transition between stability and instability, where f is the weight fraction finer than grain size d and h is the weight fraction between grain size d and $4d$. A *'f' value of* 125 μm was used during calculation of the h/f values (Table 2). The use of well graded soils means that slopes better represent more modern embankments, specifically those designed with floodwater retention in mind.

Testing processes

Following slope construction, a hydraulic head was applied to the back of the slope. Tap water was used to fill the water reservoir, which took approximately 1 min. Total seepage durations and head values used are displayed in Table 1. A constant head was used during seepage. A hydraulic gradient of 1 was used on slopes B, C and E, and a hydraulic gradient of 3 was used on slopes A and D to accelerate particle movement; higher hydraulic gradients were not used in all tests due to the potential for uplift pressures to cause instability. Hydraulic gradients were measured as the ratio of the height of the slope to the height of the water in the water reservoir. All tests were planned to run for a minimum total of 480 min of seepage time. In tests where slope failure occurred, seepage was halted at the onset of failure to preserve the remaining slope material. Failure was considered to have occurred when there was surface water flow which caused incision into the slope surface and debris flow development.

Samples were taken from slopes immediately following seepage and draining. During sampling, material was taken from sampling zones approximately 40 mm wide, 40 mm deep and 40 mm high; the location of the centre of each sampling zone is labelled in Figs. 3 and 4. For slopes A-D, the sampling zone centres were approximately 50 mm and 100 mm apart in the vertical and horizontal directions, respectively. In slope E, the centres of sampling zones were 50 mm apart in both the horizontal and vertical orientations. Material was sampled from three slope

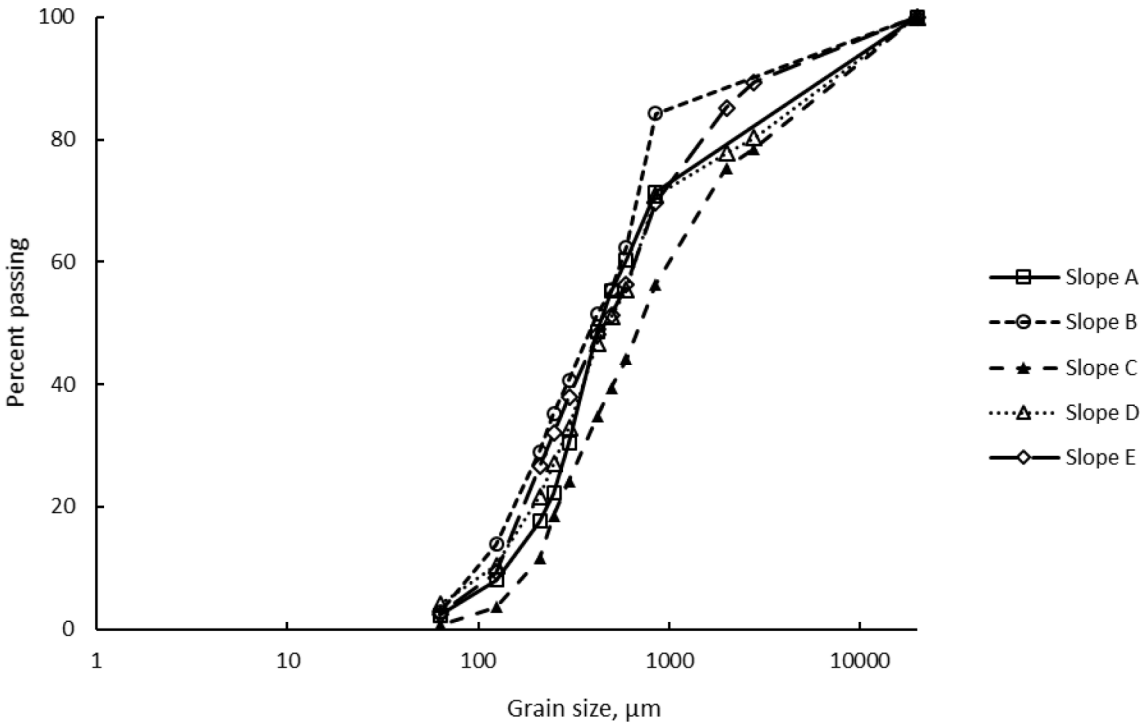

Fig. 2. Grain size distribution of soil material used during slope construction.

Table 2
Slope material stability criteria. Materials with h/f values >1.3 are considered stable. 'f' fraction relates to material <125 µm.

Slope	*Cu*	*Cc*	Kenny – Lau *h/f* ratios (1985)	*'f' Fraction*
A	6.8	1.3	2.4	8.0
B	9.9	1.1	2.1	12.8
C	7.5	0.9	1.8	11.6
D	6.5	1.0	1.7	10.4
E	5.8	1.1	1.5	9.3

transects in slopes A and B, four transects in slope C, two transects in slope D and one transect in slope E (Table 1, Figs. 3 and 4). In slopes A and B, material was sampled from four zones in the basal sampling layer, three zones in the central sampling layer and two zones in the upper sampling layer for each transect, creating a total of 9 sampling zones per transect. In slopes C and D, material was sampled from five zones in the basal sampling layer, three zones in the central sampling layer and two zones in the upper sampling layer for each transect, creating a total of 10 sampling zones per transect. In slope E, 24 samples were taken from a single transect to obtain higher resolution results – samples were taken from four vertical sampling layers; nine horizontal sampling zones were used in the lowest layer, reducing by two for each layer above (Figs. 3 and 4). The slope toe region comprises all sampling zones at a horizontal distance of 35 cm or greater.

Samples were initially taken from the top layer of slopes, before remaining material from the sampled layer was removed and the samples were taken from the layer below. Of the two transects in slope D, one was a control section which comprised a transect of the slope sampled without undergoing seepage; the second transect was sampled after undergoing seepage. After drying, the grain size distribution was measured for each sample by sieving using 12 size grading bands. *Cu*, *Cc* and average grain size values were calculated for each sample; average grain size for each sample was taken as the geometric mean, after Shirazi and Boersma (1984). A small amount of mass at higher grain sizes can have a disproportionally large effect on the results if an arithmetic mean value is taken. Fines were non-plastic so fines loss during sieving through fine particle conglomeration or fine particle attachment to coarser particles is thought to be minimal; this was confirmed by microscope analysis of the sieved particles.

Results

Here, the assumption is made that areas where mean grain size is smaller (fining of material) coincide with locations where fine particles accumulated, or coarse particles eroded, while locations with larger mean grain size indicate that fine particles were removed, or coarse particles were deposited, in that section of a slope. Grain size distribution (Fig. 3) and *Cc* (Fig. 4) data suggest that the predominant locations of changes in material properties were along the base of slopes and the sections of slopes adjacent to the water inflow. Although these patterns were seen across all slopes, they were most clearly observed in slope E which had a higher sampling resolution (Fig. 3E, 4E). Grain size distribution across each slope can be split into two broad categories. In the first, as measured in slope E and transects of slope A, B and C, higher mean grain size values were measured along the section of the slope adjacent to water inflow and along the base of the slope, with finer mean grain sizes at the toe of the slope (Fig. 3). In the second category, the toe of the slope and the section of the slope adjacent to water inflow had higher grain sizes with comparatively lower mean grain size measured along the central section of the lowest sampling layer – e.g. in slope transect *D-ii* (Fig. 3).

The combined average grain size behaviour for all slope transects (Fig. 5a) shows that a consistent trend in particle movement and deposition occurred across all slopes. Average grain sizes in Fig. 5a were obtained by first calculating the geometric mean grain size for each transect and then taking the arithmetic mean of these values for each sampling zone, not including control sections. Average grain size mean of the slope toe region was 4.5% smaller across all non-control slope transects than in the slope body (Fig. 5a), indicating that fine particle accumulation had occurred in the toe region. The 4.5% change in grain size in the slope toe region is greater than the 3% variability seen between all data points. Fining of the slope toe region is also shown in average grain size data for slopes A and B (Fig. 5c and 5d). Similar fining

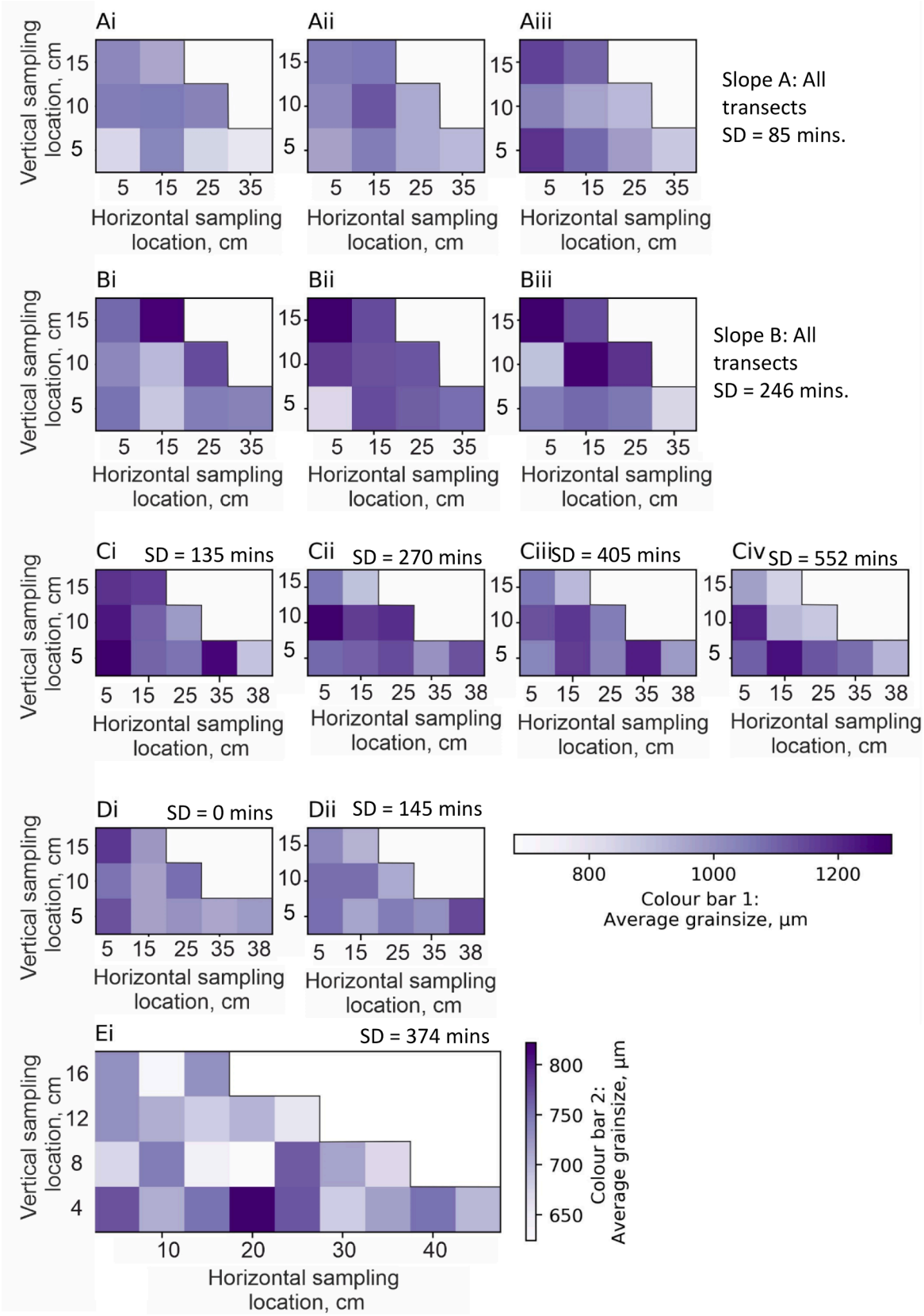

Fig. 3. Geometric mean grain size values for slopes A - E. Colour bar 1 is used for slopes A - D, colour bar 2 refers to slope E. In slope C, transect c-i underwent the shortest duration of seepage. Transect D-i was a control transect and underwent no seepage. Axes indicate where within slopes samples were taken from. SD = seepage duration. Axis distance values relate to centre of sampling zones. Dashed line represents estimated phreatic surface in relation to sampling zones.

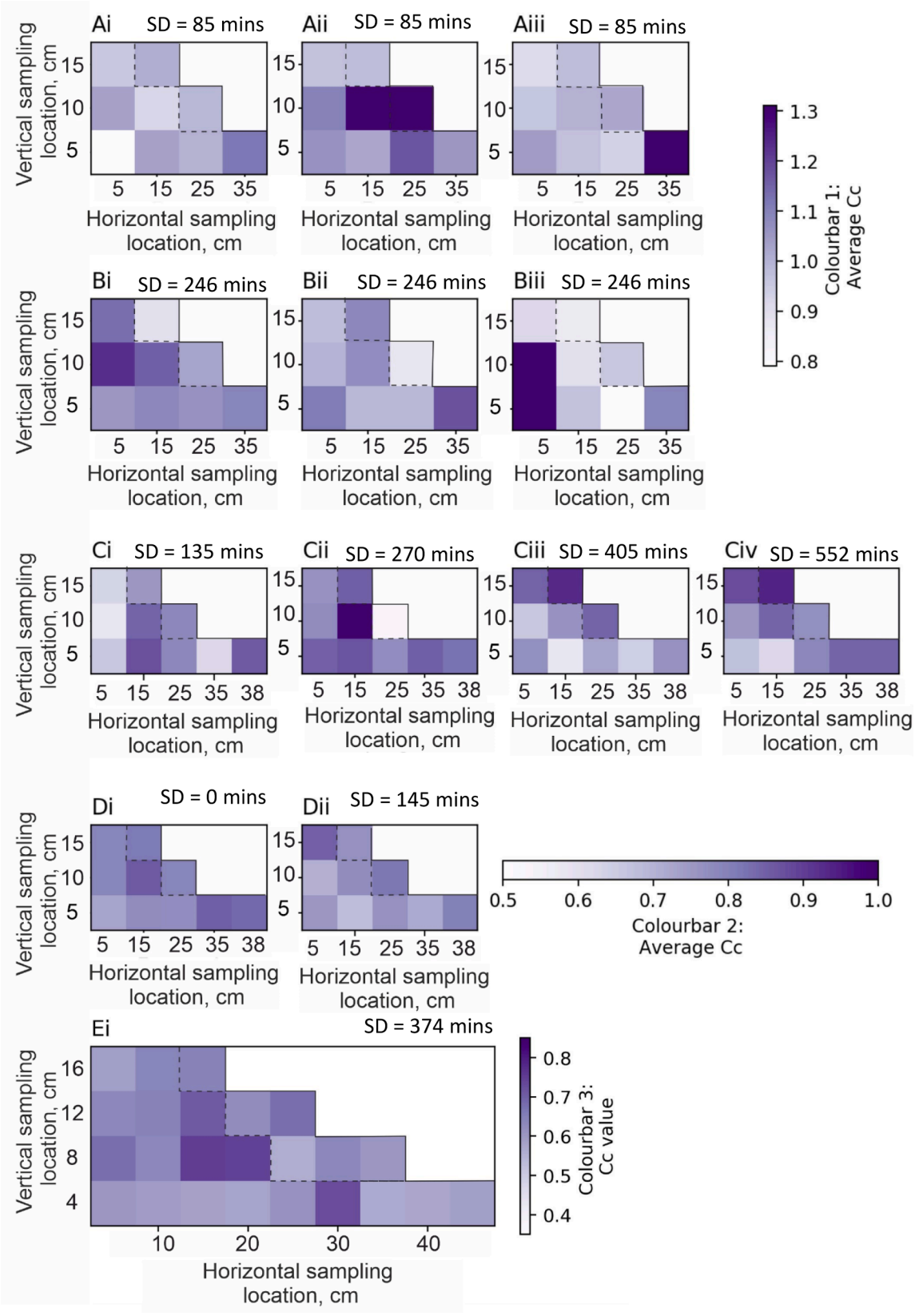

Fig. 4. Mean Cc value for each sampling point in slopes A - E. In slope C, transect (i) underwent the shortest duration of seepage and transect (iv) had longest seepage duration. Transect D-i was a control transect and underwent no seepage. Colour bar 1 refers to slope A, colour bar 2 to slopes B - D and colour bar 3 to slope E. Axis distance values relate to centre of sampling zones. Dashed line represents estimated phreatic surface in relation to sampling zones.

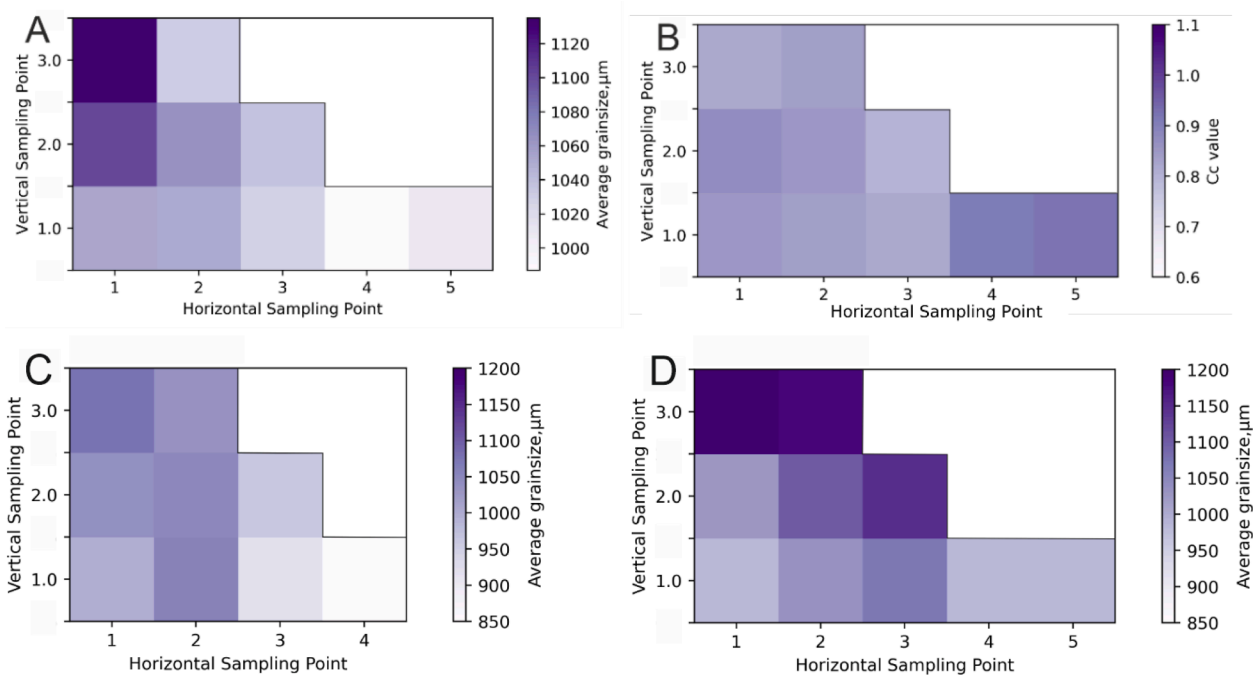

Fig. 5. Mean grain size (a) and normalised mean Cc values (b) at each sampling point for all transects of slopes A-D, excluding the control transect D-i which did not undergo seepage. (c) and (d) show mean grain size data from all transects of slopes A and B, respectively. Average grain size values for each sampling cell show the mean of the geometric mean grain size of each transect.

patterns in the slope toe are observed in slopes with hydraulic gradients of 1 and 3 – suggesting that similar seepage patterns developed in models with differing hydraulic gradients (Table 1). Although the base of slopes predominantly showed higher mean grain sizes than sampled layers above, indicating that fine particles had been removed, at the toe of slopes mean grain sizes were predominantly lower relative to values along the base of the slope (e.g. transects *B-iii* and *C-iv*). Across all slopes, a consistent trend in average grain size behaviour was not as well defined in the upper right sections of slopes, which was thought to be above the phreatic surface – meaning there would have been little to no seepage through this material.

In slopes D and E, the mean grain size for each sampling layer (geometric mean of each horizontal layer) shows that the top half of the slope had a constant average grain size and in the bottom sampling layers the mean grain size increased (Fig. 6). Increases of 17.5% were observed in the lowest layer in transect *D-ii* and 12.5% across the lowest two sampling layers in transect *E-i.* This pattern was not observed in the control transect of slope D (*D-i*), which had a maximum measurement range of 3.7% between sampling layers; as transect *D-i* was sampled without undergoing seepage this suggests the variance observed in transect *D-i* was caused by slope inhomogeneity. Accounting for the inherent inhomogeneity from slope construction, increases of 13.7% and 9.7% are thought to have developed due to seepage-induced particle migration in transects *D-i* and *E-i*, respectively.

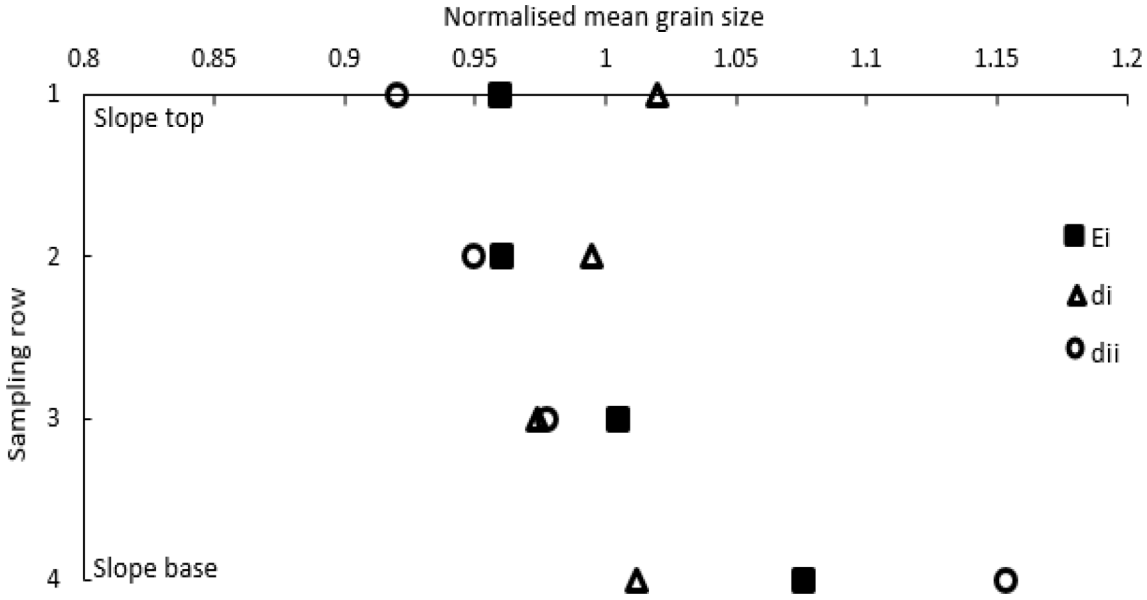

Fig. 6. Normalised mean grain size for each horizontal layer in slopes D and E. Transect 'D-i', was a control section, sampled without seepage. Values normalised by the geometric mean grain size of each transect.

Distinct *Cc* patterns were observed in slopes C, D and E (Fig. 4). In slope transects *B-i, B-ii, C-iv, D-ii* and *E-i* low *Cc* values were observed in the basal slope layer relative to higher sampling layers, with the exception of the slope toe. In slope C, in the slope section adjacent to water inflow, *Cc* values were lowest following the initial stage of seepage (transect *C-i*), and increased with further seepage. Along the base of slope C, *Cc* values increased after the initial stages of seepage (*C-ii*), then predominantly decreased with time — excluding in the slope toe region (*C-iii* and *C-iv*) (Fig. 4c). Normalised average *Cc* values for all tests, normalised by the average *Cc* value of all samples in slopes A-D combined, showed distinctly higher *Cc* values in the slope toe region (Fig. 5b). Higher *Cc* values recorded at the toe of the slope indicate that the material became better graded, which is consistent with fine particle deposition. Areas with lower *Cc* values indicate that the slope-forming materials were more poorly graded. Across all tests, no spatial or temporal behavioural trends were observed in *Cu* data, suggesting that there was not a distinct effect of fine particle migration on the *Cu* values. Mean post-seepage *Cc* values for all transects of slopes A-E were: 1.27, 0.75, 0.77, 0.78 and 0.63, respectively. Mean post seepage *Cc* values for each slope were lower than the initial Cc values for the initial soil mixes (Table 2). Post seepage mean *Cc* values were higher for slope A than for the other model slopes.

In slope C, in the transect sampled after the first stage of seepage, average grain size values were initially higher at the head of the slope relative to the rest of the slope, with larger fines content at the slope toe. Samples from transects *C-ii, C-iii and C-iv,* which were subjected to progressively greater seepage volumes, show that the toe of the slope coarsened before fining again, while towards the head of the slope the material initially fined and then became coarser. Temporal development of slope properties was also observed in slope D, in which there was a decrease in mean grain size in the slope area adjacent to water inflow and increase in grain size along the base and toe of the slope with time.

Little variation was observed in the properties of materials in the upper right portion of slopes. Furthermore, a fine-grained zone was observed in the bottom left corner and slope toe region of transects *A-i* and *A-ii*; (Fig. 7). In slope transect *A-i*, the fine particle accumulation was visible at the toe of the slope after 75 min of seepage (Fig. 7), consistent with the observed fluorescence development through the slope and lower mean grain size values measured in this region. Fine-grained material was observed exiting the toe of slopes with seepage progression in all slopes. Fluorescence migration through slopes primarily displayed movement towards the slope toe and downwards towards the slope base from the input locations. Fluorescence migration was more obvious in the lower sections of slopes, consistent with locations of observed spatial trends in *Cc* and mean grain size data. In slope A, fluorescent water can be seen rising over the zone of fines deposition at the slope toe (Fig. 7). Debris flow failures initiated in the upper sections of slopes A, B and D. In slope C, a rotational failure initiated in the middle of the slope. These tests were halted at this point to preserve the remaining material for sampling. Material altered by failure was not sampled.

Discussion

Observed spatial patterns in mean grain size and *Cc* data are consistent with the migration of fine particles, driven by water inflow at the back of the slope, from the rear of the slope towards the slope toe, with movement primarily occurring along the basal sampling layer of the samples. These findings are broadly consistent with previous model slope tests which used bi-modal silica as a soil substitute (Horikoshi and Takahasi, 2015). The highest mean grain sizes were most commonly measured along the base and at the rear of the slope, suggesting that fine particle removal occurred from those areas. Low average grain sizes were most commonly found in the toe of the slope, consistent with fine particle deposition in this area. Higher *Cc* values, suggesting a better graded soil, at the toe of the slope also support the suggestion that there was migration of fine particles towards the slope toe, with the source regions being the back of the slope and slope base. Post seepage *Cc* values are lower than the initial values for the bulk soil mixture for all slopes (Table 2). Smaller Cc reductions in slope in slope A are attributed to the shorter seepage duration for the slope, limiting the number of fine particles removed from the slope. The deposition of fine particles in the downstream section, specifically the toe region of the slope, has the potential effect of reducing permeability [7] and increasing pore water pressures; these changes may reduce slope stability when applied to larger embankments. Fluorescein flow over the top of the fine particle accumulation zone in the slope toe (Fig. 7) provides qualitative evidence for the development of an area of lower permeability. If fine particles are lost from an area of a slope, material permeability may increase. Permeability increases have the potential to reduce the susceptibility of a material to the effects of rapid drawdown, as pore water pressures will dissipate more quickly during the drawdown process [24], increasing slope stability. Conversely, increases in surface permeability, which controls water infiltration into a slope [11], are capable of increasing

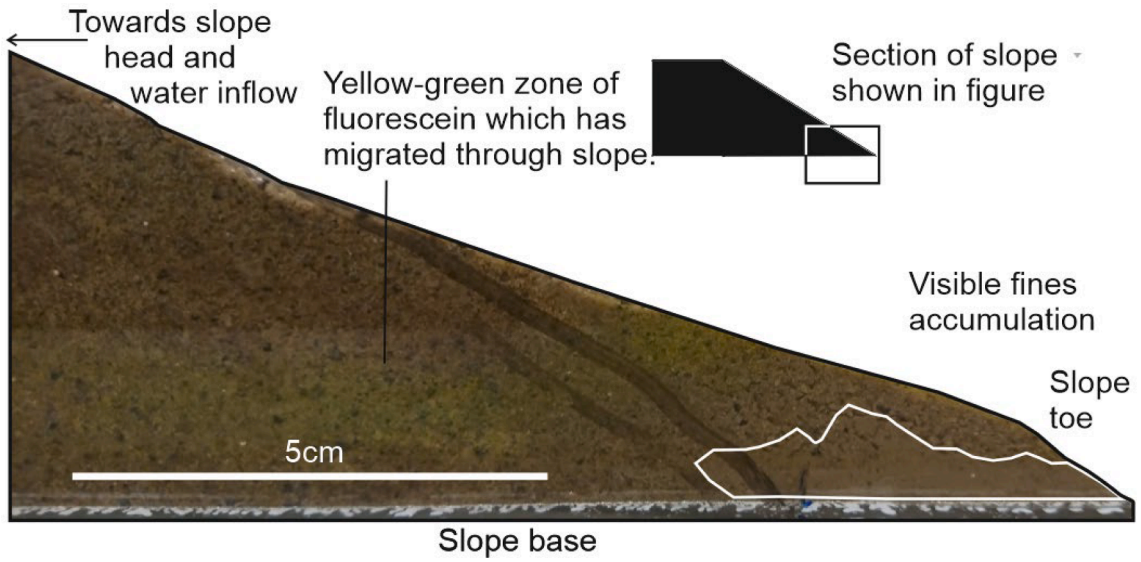

Fig. 7. Fine particle accumulation at the toe of slope 'A'. Fluorescein migration is also evident, with a fluorescent zone visible above the zone with fine particle deposition.

water infiltration from flooding or rainfall — potentially causing destabilisation through increases in pore water pressures.

In some tests, higher mean grain sizes were observed in the slope toe region than for the remainder of the slope base, e.g. in transects *D-ii* and *C-ii*. This is thought to be due to shorter durations of seepage in these tests and the removal of mobilised loose fine particles from the slope toe during early seepage — but without enough seepage volume to move additional fine particles washed out from the back of the slope into the terminal slope sections. Loose particle migration at the onset of seepage, followed by coarser particle movement and macropore development, is consistent with the expected behaviour of unstable granular soils [8]. In addition to the aforementioned seepage-driven directional movement of fine particles, the development of zones with locally increased grain sizes along the base of slope *A* is thought to have been caused by deposition of fine particles behind impermeable berms and the removal of such particles from in front of them. Higher mean grain sizes in the slope regions closest to water inflow and in the lowest sampling sections of slopes, e.g. slope *E*, (Figs. 3, 5a) suggest that the majority of fine particles deposited in the toe or washed out of slopes are sourced from these regions.

Under the effects of seepage, the localised movement and redistribution of fine particles, initially located in inter-granular zones, into constrictions at inter-particle contacts, is thought to have an important effect on the mechanical behaviour of slopes [2]. Although the particles mobilised are not removed from the slope during this localised redistribution, the restructuring of the soil alters the material behaviour. As particles are not removed from the slope during localised redistribution, average grain size, *Cc* or *Cu* will be consistent with pre-seepage values at the slope scale. The permeability reductions associated with the movement of fine particles from head to toe of slopes and accumulation of fine particles at interparticle contacts are potential causative factors for the formation of failure events observed during the latter stages of flow during testing. If extrapolated to larger-scale slopes, as found in infrastructure earthworks, these changes have the potential to cause long-term degradation of slopes and associated destabilisation; material changes may not be observable without intrusive investigation. Although the authors are not aware of studies on full-scale embankments undertaken to assess the effects of flooding on particle migration, there is plentiful evidence available of subsurface sediment removal from slopes (e.g. [1,31,5,20,9]).

Although the laboratory model used in the testing is thought to be a good proxy for assessing the potential for changes in full-scale embankment properties caused by water impoundment and seepage throughflow, boundary effects may have altered the primary flow pathway. Additionally, the impermeable base prevented the movement of water and fine particles out of the slope base. The permeability barrier formed by the soil-box base contact may exacerbate the role of basal flow in these tests, making them more representative of scenarios where embankments overlie impermeable soils or bedrock. However, it is evident from the primary trends in *Cc* and mean grain size data that the most property alteration is likely to occur in these lower slope regions. Due to the time-dependent nature of the effects of seepage on slopes, it is difficult to specify the exact property changes that would develop in full-scale embankments after a specific flooding event as they may be dependent on factors including the head of water, previous slope alteration and duration of the specific flooding process in question [13]. We found that, during initial seepage, fine particles are lost from the slope toe region; deposition subsequently occurs in this area due to particle migration from upstream sections of a slope.

Geometric mean grain size and *Cc* were found to display the most obvious patterns of material behaviour following seepage; no distinct spatial or temporal pattern was observed in *Cu* data. Based on these results, *Cc* and geometric mean grain size change are thought to be the most reliable measure for assessing changes in the behaviour of materials following seepage development. It is thought that *Cu* values are not consistently altered by the migration of fine particles as the movement of fine particles has more effect on D_{10} and D_{30}, which have a greater control on *Cc* than *Cu,* than on D_{60}. The patterns of material alteration, likely caused by the redistribution of fine particles, identified in our experiments suggest that funding should be invested to examine the scale of slope alteration following flooding in full-scale embankment slopes.

Conclusion

Seepage through scale model slopes caused material property differences along the slope profile relative to the control slope where no differences were observed across the slope profile. The spatial differences were observed in geometric mean grain size and *Cc* data. Larger mean grain sizes were primarily observed at the base and back of slopes, suggesting that fine particle loss occurred. Smaller mean grain sizes were most commonly found at the toe of slopes, suggesting fine particle deposition occurs in these areas. The movement of fine particles appeared to be time dependent. Initial short durations of seepage may remove fine particles from some areas, such as the slope toe, before additional seepage causes deposition of fine particles sourced from upstream sections of slopes. Reduction in average grain size, and associated fine particle deposition, at the toe of slopes has the potential to reduce overall slope permeability and may cause slope destabilisation. This potential for slope destabilisation suggests the need for investment in larger-scale analysis of embankment slopes affected by flooding.

CRediT authorship contribution statement

I. Johnston: Conceptualization, Methodology, Data curation, Formal analysis, Investigation, Visualization, Writing – original draft, Writing – review & editing. **W. Murphy:** Supervision, Methodology, Conceptualization, Writing – review & editing. **J. Holden:** Supervision, Methodology, Conceptualization, Writing – review & editing.

Declaration of Competing Interest

The authors declare that they have no known competing financial interests or personal relationships that could have appeared to influence the work reported in this paper.

Data availability

Data will be made available on request.

Acknowledgements

This research was funded by the UK Natural Environment Research Council and Network Rail as part of the National Productivity Investment Fund award number NE/R009813/1. Laboratory testing was undertaken in the RMEGGh laboratories at the University of Leeds; Kirk Handley is thanked for his assistance during the set-up and design of laboratory testing.

References

[1] Ahmed AAA, Joudah AA. Review About Incidents in Dams and Dike Behaviours Induced by Internal Erosion. Int J Eng Technol (IRJET) 2021;8:1057–513.
[2] Alramahi B, Alshibli KA, Fratta D. Effect of Fine Particle Migration on the Small-Strain Stiffness of Unsaturated Soils. J Geotech Geoenviron Eng 2010;136:620–8.
[3] ASCE. Earthen Embankment Breaching. J Hydraul Eng 2011;137:1549–64.
[4] Bennett EH. Court of Appeal. Whalley v. Lancashire and Yorkshire Railway Co. The American Law Register (1852-1891), 1884; 32: 633-640.
[5] Bernatek-Jakiel A, Poesen J. Subsurface erosion by soil piping: significance and research needs. Earth Sci Rev 2018;185:1107–28.
[6] Chang D, Zhang L. A Stress-controlled Erosion Apparatus for Studying Internal Erosion in Soils. Geotech Test J 2011;34:579–89.
[7] Chang DS, Zhang LM. Critical Hydraulic Gradients of Internal Erosion under Complex Stress States. J Geotech Geoenviron Eng 2013;139:1454–67.

[8] Chang DS, Zhang LM. Extended internal stability criteria for soils under seepage. Soils Found 2013;53:569–83.
[9] Ferdos F. Internal Erosion Phenomena in Embankment Dams: Throughflow and internal erosion mechanisms; 2016.
[10] Field CB, Barros V, Stocker TF, Dahe Q. Managing the risks of extreme events and disasters to advance climate change adaptation: special report of the intergovernmental panel on climate change. Cambridge University Press; 2012.
[11] Gavin K, Xue J. A simple method to analyze infiltration into unsaturated soil slopes. Comput Geotech 2008;35:223–30.
[12] Horikoshi K, Takahashi A. Suffusion-induced change in spatial distribution of fine fractions in embankment subjected to seepage flow. Soils Found 2015;55:1293–304.
[13] Johnston I, Murphy W, Holden J. A review of floodwater impacts on the stability of transportation embankments. Earth Sci Rev 2021;215:103553.
[14] Ke L, Takahashi A. Strength reduction of cohesionless soil due to internal erosion induced by one-dimensional upward seepage flow. Soils Found 2012;52:698–711.
[15] Ke L, Takahashi A. Experimental investigations on suffusion characteristics and its mechanical consequences on saturated cohesionless soil. Soils Found 2014;54:713–30.
[16] Kelly D, McDougall J, Barreto D. In: Effect of particle loss on soil behaviour. Paris: Publications SHF; 2012. p. 639–46.
[17] Kenney T, Lau D. Internal stability of granular filters. Can Geotech J 1985;22:215–25.
[18] Kwan WS, Mohtar CE. A review on sand sample reconstitution methods and procedures for undrained simple shear test. Int J Geotech Eng 2018;14:1–9.
[19] Luo Y-L, Qiao L, Liu X-X, Zhan M-L, Sheng J-C. Hydro-mechanical experiments on suffusion under long-term large hydraulic heads. Nat Hazards 2013;65:1361–77.
[20] Maknoon M, Mahdi T-F. Experimental investigation into embankment external suffusion. Nat Hazards 2010;54:749–63.
[21] Menan Hasnayn M, John Mccarter W, Woodward PK, Connolly DP, Starrs G. Railway subgrade performance during flooding and the post-flooding (recovery) period. Transp Geotech 2017;11:57–68.
[22] Mossa M. The floods in Bari: What history should have taught. J Hydraul Res 2007;45:579–94.
[23] Peterson C. pH Dependence and Unsuitability of Fluorescein Dye as a Tracer for Pesticide Mobility Studies in Acid Soil. Water Air Soil Pollut 2010;209:473–81.
[24] Pinyol NM, Alonso EE, Olivella S. Rapid drawdown in slopes and embankments. Water Resour Res 2008;44:W00D03.
[25] Polemio M, Lollino P. Failure of infrastructure embankments induced by flooding and seepage: a neglected source of hazard. Nat Hazards Earth Syst Sci 2011;11:3383.
[26] Sato M, Kuwano R. Effects of internal erosion on mechanical properties evaluated by triaxial compression tests. Japanese Geotechnical Society Special Publication 2016;2:1056–9.
[27] Stirling RA, Toll DG, Glendinning S, Helm PR, Yildiz A, Hughes PN, et al. Weather-driven deterioration processes affecting the performance of embankment slopes. Géotechnique 2021;71:957–69.
[28] Tsubaki R, Kawahara Y, Ueda Y. Railway embankment failure due to ballast layer breach caused by inundation flows. Nat Hazards 2017;87:717–38.
[29] UIC. UIC Leaflet 719R: Earthworks and track bed for railway lines. 3rd ed. International Union of Railways; 2008.
[30] USBR 2015. Best Practices in Dam And Levee Safety Risk Analysis. 4th ed.
[31] Wan CF, Fell R. Investigation of internal erosion by the process of suffusion in embankment dams and their foundations. Internal erosion of dams and their foundations. CRC Press; 2007.
[32] Wan CF, Fell R. Assessing the Potential of Internal Instability and Suffusion in Embankment Dams and Their Foundations. J Geotech Geoenviron Eng 2008;134:401–7.